Pauli energy contribution to nucleus-nucleus interaction

A.S. Umar[1,⋆], *K.* Godbey[2,⋆⋆], and *C.* Simenel[3,⋆⋆⋆]

[1] *Department of Physics and Astronomy, Vanderbilt University, Nashville, TN 37235, USA*
[2] *Facility for Rare Isotope Beams, Michigan State University, East Lansing, Michigan 48824, USA*
[3] *Department of Fundamental and Theoretical Physics and Department of Nuclear Physics and Accelerator Applications, Research School of Physics, The Australian National University, Canberra ACT 2601, Australia*

Abstract. The investigation delves into understanding how the Pauli exclusion principle influences the bare potential between atomic nuclei through the application of advanced theoretical methodologies. Specifically, the application of the novel Frozen-Hartree-Fock (DCFHF) technique is employed. The resulting potentials demonstrate a noticeable repulsion at short distances, attributed to the effects of the Pauli exclusion principle. To account for dynamic phenomena, such as nucleon transfer processes, the density-constrained time-dependent Hartree-Fock (DC-TDHF) method is utilized. This approach integrates isovector contributions into the potential, shedding light on their influence on fusion reactions. Notably, the inclusion of isovector effects leads to a reduction or enhancement in the inner part of the potential, suggesting a nuanced role of transfer in the fusion process.

1 Introduction

The Pauli exclusion principle plays a crucial role as a building block of many-body quantal systems comprised of fermions. It also induces a "Pauli repulsion" in the interaction between di-nuclear systems. It has been shown that [1] the Pauli repulsion widens the nucleus-nucleus potential barrier, thus hindering sub-barrier fusion. We investigate the proton and neutron contributions to the Pauli repulsion, both in the bare potential neglecting shape polarization and transfer between the reactants, as well as in the dynamical potential obtained by accounting for such dynamical rearrangements. As the basis of our study we utilize the Pauli kinetic energy (PKE) obtained by studying the nuclear localization function (NLF) [2]. Recently this approach has been generalized to incorporate all of the dynamical and time-odd terms present in the nuclear energy density functional [3]. This approach is employed in the density constrained frozen Hartree-Fock (DCFHF) and in the density constrained time-dependent Hartree-Fock (DC- TDHF) microscopic methods. The PKE spatial distribution shows that a repulsion occurs in the neck between the nuclei when they first touch. Inside the barrier, neutrons can contribute significantly more to the Pauli repulsion in neutron-rich systems. Dynamical effects tend to lower the Pauli repulsion near the barrier. Proton and neutron dynamical contributions to the PKE significantly differ inside the barrier for asymmetric collisions, which is interpreted as an effect of multinucleon transfer. The PKE is shown to make a significant contribution to nuclear interaction potentials. Protons and neutrons can play very different roles in both the bare potential and in the dynamical rearrangement. Further microscopic studies are required to better understand the role of transfer and to investigate the effect of pairing and deformation [4].

⋆e-mail: umar@compsci.cas.vanderbilt.edu
⋆⋆e-mail: kylegodbey@gmail.com
⋆⋆⋆e-mail: cedric.simenel@anu.edu.au

2 Formalism

2.1 Microscopic Methods

To explore the influence of the Pauli energy in heavy-ion fusion reactions, our methodology incorporates microscopic techniques to calculate the interactions between nuclei. We base our approach on the energy density functional (EDF) to compute nucleus-nucleus potentials. The computation of the bare potential begins with the assumption of frozen ground-state densities for each nucleus, derived from the Hartree-Fock (HF) mean-field approximation. This method leverages the Skyrme EDF for both the HF calculations and the potential computation, ensuring consistency without introducing additional parameters. This potential is derived from the spatial integral of the energy density as a function of the nuclear densities

$$V_{\rm FHF}(\mathbf{R}) = \int d\mathbf{r}\, \mathcal{H}\left[\rho_1(\mathbf{r}) + \rho_2(\mathbf{r}-\mathbf{R})\right] - E[\rho_1] - E[\rho_2]\,. \tag{1}$$

Here, Pauli exclusion principle's effects are initially set aside, except for those emanating from the exchange terms in the effective interaction, leading to the formulation of the conventional FHF potential [5–10].

To incorporate the Pauli repulsion into the bare potential, we adopt the DCFHF method [1]. This approach includes the Pauli exclusion principle explicitly by allowing

the reorganization of single-particle states within the combined nuclear density to achieve a minimum energy configuration. This reorganization results in a unique Slater determinant, with the HF minimization performed under constraints that maintain the local densities of protons and neutrons unchanged

$$\delta\left\langle H - \sum_{q=p,n}\int d\mathbf{r}\,\lambda_q(\mathbf{r})\left[\rho_{1_q}(\mathbf{r}) + \rho_{2_q}(\mathbf{r}-\mathbf{R})\right]\right\rangle = 0\,. \quad (2)$$

The DCFHF method yields bare potentials that acknowledge the Pauli repulsion, effectively widening the fusion barrier and generating a potential pocket at closer distances not observed in FHF potentials

$$V_{\mathrm{DCFHF}}(R) = \langle\Phi(\mathbf{R})|H|\Phi(\mathbf{R})\rangle - E[\rho_1] - E[\rho_2]\,. \quad (3)$$

This difference enables a comparative study of the Pauli principle's impact on frozen nuclear densities.

For dynamic nuclear interactions, we turn to the time-dependent Hartree-Fock (TDHF) calculations. These calculations consider the rearrangement of densities at the mean-field level, affected by couplings to vibrational and rotational modes, as well as nucleon transfer mechanisms. The potentials derived from TDHF calculations, therefore, reflect both dynamical effects and the Pauli exclusion principle. To delve deeper into these dynamics, we employ the Density-Constrained TDHF (DC-TDHF) method, directly using the densities from TDHF system evolution while applying the same constraint procedure as in DCFHF

$$V_{\mathrm{DC-TDHF}}(R) = \langle\Phi(\mathbf{R}(\mathbf{t}))|H|\Phi(\mathbf{R}(\mathbf{t}))\rangle - E[\rho_1] - E[\rho_2]\,. \quad (4)$$

The DC-TDHF approach [7,9,11–13] allows for a nuanced understanding of microscopic phenomena related to the Pauli principle, including orbital splitting and its attractive or repulsive contributions to the potential. However, it's crucial to note the inherent limitations of TDHF-based methods, such as their inability to account for many-body tunneling effects, which leaves the energy dependency of the potential at sub-barrier energies as an open question. Despite these limitations, the application of DC-TDHF potentials in calculating near- and sub-barrier fusion cross-sections has demonstrated considerable success in aligning with experimental outcomes, showcasing the method's efficacy in capturing the complex interplay of nuclear forces at play in heavy-ion fusion reactions.

2.2 Localization function and PKE

This section delves into the concept of the localization function for nuclear systems [2,3] and its connection to kinetic energy and the Pauli exclusion principle. The conditional probability for finding a nucleon at $\mathbf{r}'$, shown in Fig. 1, when we know with certainty that another nucleon with the same spin and isospin is at $\mathbf{r}$ is proportional to

$$R_{qs}(\mathbf{r},\mathbf{r}') = \frac{\rho_q(\mathbf{r}s,\mathbf{r}s)\rho_q(\mathbf{r}'s,\mathbf{r}'s) - |\rho_q(\mathbf{r}s,\mathbf{r}'s)|^2}{\rho_q(\mathbf{r}s,\mathbf{r}s)}\,, \quad (5)$$

where ρ_q is the component of the one-body density matrix with isospin q.

The short-range behavior of R_{qs} can be obtained using techniques similar to the local density approximation [2,3]. The leading term in the expansion yields the localization measure

$$D_{qs_\mu} = \tau_{qs_\mu} - \frac{1}{4}\frac{\left|\boldsymbol{\nabla}\rho_{qs_\mu}\right|^2}{\rho_{qs_\mu}} - \frac{\left|\mathbf{j}_{qs_\mu}\right|^2}{\rho_{qs_\mu}}\,, \quad (6)$$

where the densities and currents are given in their most unrestricted form [3] for μ axis denoting the spin-quantization axis. This measure is the most general form

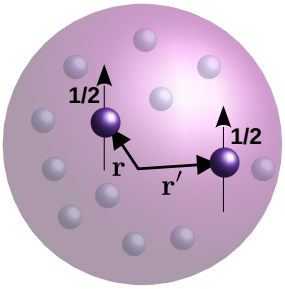

Figure 1. Schematic depiction of two nucleons at $\mathbf{r}$ and $\mathbf{r}'$ with spin up along the z-axis entering Eq. (5).

that is appropriate for deformed nuclei and without assuming time-reversal invariance, thus also including the time-odd terms important in applications such as cranking or TDHF. We can visualize the NLF defined from the localization measure in Eq. (6). It is advantageous to normalize the localization measure to the interval [0, 1] using [3,14]

$$\mathcal{D}_{qs_\mu}(\mathbf{r}) = \frac{D_{qs_\mu}(\mathbf{r})}{\tau^{\mathrm{TF}}_{qs_\mu}(\mathbf{r})}\,, \quad (7)$$

where the normalization $\tau^{\mathrm{TF}}_{qs_\mu}(\mathbf{r}) = \frac{3}{5}\left(6\pi^2\right)^{2/3}\rho^{5/3}_{qs_\mu}(\mathbf{r})$ is the Thomas-Fermi kinetic density. The NLF can then be represented by

$$C_{qs_\mu}(\mathbf{r}) = \left[1 + \mathcal{D}^2_{qs_\mu}\right]^{-1}\,. \quad (8)$$

To calculate the Pauli kinetic energy the expression in Eq. (6) can be dissected into two components. The last two terms are the kinetic density for a complex valued single particle state of a given spin s and isospin q. The first term represents the von Weizsacker kinetic-energy density, and together, these provide the kinetic density [3]

$$\tau^{\mathrm{s.p.}}_{qs} = \frac{1}{4}\frac{\left|\boldsymbol{\nabla}\rho_{qs}\right|^2}{\rho_{qs}} + \frac{\left|\mathbf{j}_{qs}\right|^2}{\rho_{qs}}\,. \quad (9)$$

Thus, one can write

$$D_{qs} = \tau_{qs} - \tau^{\mathrm{s.p.}}_{qs}\,. \quad (10)$$

This equation establishes D_{qs} as the difference between the total kinetic energy density and the kinetic energy density for a single-particle state, being zero for a single nucleon system. D_{qs} directly measures the additional kinetic density brought about by the Pauli exclusion principle, which

prevents two fermions (such as protons or neutrons in a nucleus) from occupying the same quantum state. The total PKE for a nuclear system can be obtained by integrating

$$E^{\mathrm{P}}_{qs} = \frac{\hbar^2}{2m} \int d^3r \, D_{qs}(\mathbf{r}) \,. \tag{11}$$

Since the PKE for a single nucleus does not contribute to the Pauli repulsion for the nucleus-nucleus potential, we can define the difference

$$\Delta E^{\mathrm{P(F)}}_{q\mu}(R) = \frac{\hbar^2}{2m} \sum_{s_\mu} \int d^3r \, \left[D^{\mathrm{DCFHF}}_{qs_\mu}(\mathbf{r}, R) - D^{\mathrm{FHF}}_{qs_\mu}(\mathbf{r}, R) \right] , \tag{12}$$

where we have subtracted the contribution of the PKE from the FHF approach and summed over the spin-up and spin-down components for a given spin projection axis μ. Indeed, the latter uses the same frozen density as DCFHF, but it neglects the Pauli exclusion principle between nucleons of different nuclei. The notation P(F) stands for "Pauli in the Frozen approximation". A similar expression can be constructed by subtracting DC-TDHF and DCFHF contributions to identify the dynamical contribution to PKE.

3 Results

One of the interesting results is the observation of Pauli repulsion directly through NLF. In Fig. 2 we show the stacked plot of NLF's for neutron distributions, obtained with the DCFHF method for spin up along the z-axis, corresponding to (a) ^{40}Ca+^{40}Ca, (b) ^{48}Ca+^{48}Ca, and (c) ^{16}O+^{208}Pb. The NLF for protons is very similar to that of the neutrons. The approximate distance between the nuclei is about 11 fm. We note the effect of the Pauli repulsion on the single-particle states resulting from the DCFHF calculation, concentrating in the region of touching surfaces. We should remember that since the densities are frozen the corresponding density plots will not show any Pauli effects.

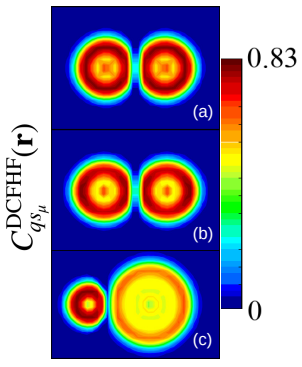

Figure 2. Plotted are the NLF's, obtained with the DCFHF method for spin up along the z-axis, corresponding to (a) ^{40}Ca+^{40}Ca, (b) ^{48}Ca+^{48}Ca, and (c) ^{16}O+^{208}Pb systems at $R \approx$ 11 fm.

The contributions of protons and neutrons to Pauli repulsion, calculated using Eq. (12) under the assumption of frozen nuclear densities, are depicted in Fig. 3 for the ^{40,48}Ca+^{40,48}Ca systems. A pronounced increase in Pauli repulsion is observed inside the barrier for all examined nuclear systems. The kinetic energy due to the Pauli principle becomes significantly large at shorter distances between the ions. This phenomenon underlies the formation of a potential well at close separations, suggesting that the increase in PKE counterbalances the rapid decrease in the interaction potentials derived from static (frozen) nuclear densities.

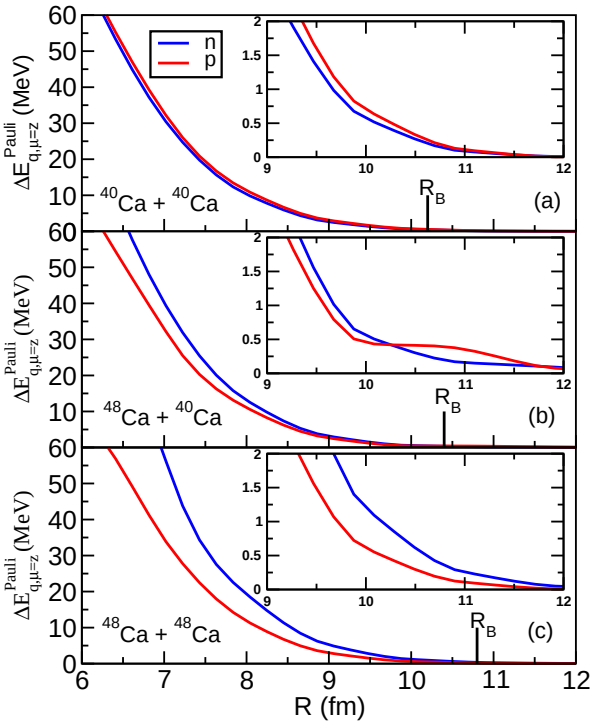

Figure 3. Neutron and proton contributions to the Pauli repulsion from Eq. (12) in the frozen approximation for the ^{40,48}Ca+^{40,48}Ca systems. The insets focus on the barrier top region.

In the system of ^{40}Ca+^{40}Ca, where the number of protons equals the number of neutrons ($N = Z$), the contributions from both protons and neutrons to the Pauli energy are almost identical. For the systems that do not have extended neutron skins the protons interact earlier due to the Coulomb interaction, which leads to an early increase for proton PKE. While the proton contribution remains relatively constant across the ^{40,48}Ca+^{40,48}Ca systems, the Pauli contribution noticeably strengthens with an increase in the neutron number within the barrier. For example, at a separation of $R \approx 9$ fm in the ^{48}Ca+^{48}Ca system, corresponding to the inner turning point of a quantum tunneling path at roughly 0.9 times the barrier potential (V_B), the contribution is predominantly exerted by neutrons. Consequently, the neutron contribution to the Pauli energy significantly surpasses the proton contribution.

A similar trend is observed in the ^{16}O+^{208}Pb system shown in Fig. 4, where the neutron contribution is roughly double that of the proton force contribution inside the barrier. This pattern may be attributed to the formation of neutron skins in neutron-rich nuclei, which results in neu-

trons interacting first near the barrier's edge. Therefore, the Pauli exclusion principle predominantly affects neutrons in such configurations. Consequently, one may expect a fusion hindrance due to the Pauli exclusion principle in neutron-rich systems, in particular at sub-barrier energies.

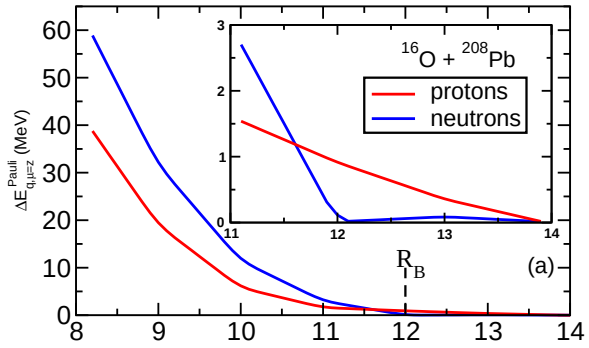

Figure 4. Neutron and proton contributions to the Pauli repulsion from Eq. (12) in the frozen approximation for the ^{16}O+^{208}Pb system. The inset focuses on the barrier top region.

In the realm of frozen density frameworks, the DCFHF approach incorporates antisymmetrization principles to yield a refined prediction of the Pauli Kinetic Energy (PKE) at a static, mean-field level. Nonetheless, a dynamic examination of nuclear reactions reveals that the densities of interacting nuclei are dynamic, engaging with each other prior to surpassing the barrier peak. This interaction leads to shape polarization and potential nucleon exchange between the fragments, while adhering to the Pauli exclusion principle. Within density functional theory (DFT), such dynamics are modeled through the TDHF (or TDDFT) evolution. The DC-TDHF method calculates the nucleus-nucleus potential based on these time-evolving densities, allowing for a nuanced comparison of Pauli repulsion effects under static and dynamic conditions, thereby enhancing our understanding of Pauli kinetic energy's dynamic development. To this end we can define a similar measure

$$\Delta E^{\mathrm{P(D)}}_{q\mu}(R) = \frac{\hbar^2}{2m}\sum_{s_\mu}\int d^3r\,\left[D^{\mathrm{DC-TDHF}}_{qs_\mu}(\mathbf{r},R) - D^{\mathrm{DCFHF}}_{qs_\mu}(\mathbf{r},R)\right]. \tag{13}$$

Figures 5 and 6 display the variance in Pauli energies as derived from DC-TDHF and DCFHF methodologies relative to the internuclear distance, R. In every instance, incorporating dynamics lowers the overall Pauli repulsion across proton and neutron contributions near the barrier radius, R_B. Given that TDHF formulations stem from a principle of stationary action, which typically minimizes action (and since a rise in PKE would increase the action), it's logical for the system to seek configurations that diminish PKE. Closer internuclear distances, however, witness a surge in total PKE. It's important to recognize that density configurations at smaller R markedly differ from static densities, making the PKE disparity at $R \leq R_B$ sometimes less significant. Nonetheless, the dynamic-induced increase in Pauli repulsion at close ranges might reflect a physical phenomenon, such as nucleon dynamical collectivization, which elevates the PKE as collision partners coalesce.

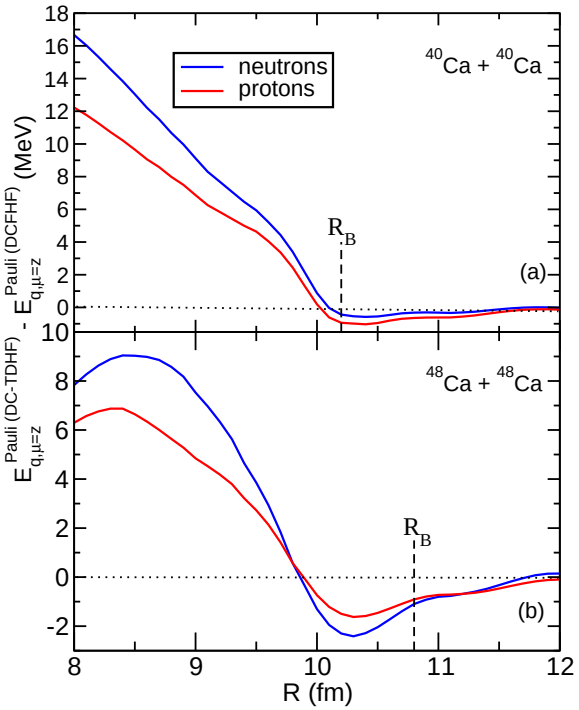

Figure 5. Dynamical contributions to the Pauli repulsion computed from Eq. (13) for the ^{40}Ca+^{40}Ca and ^{48}Ca+^{48}Ca) systems.

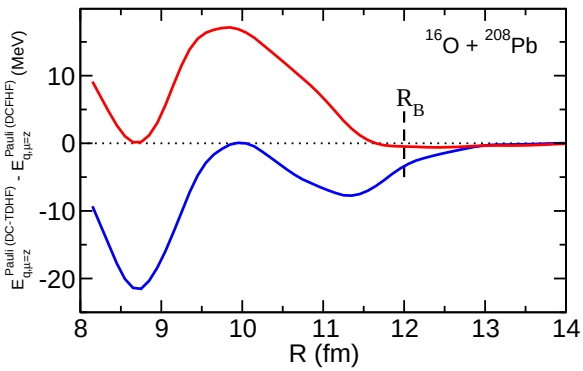

Figure 6. Dynamical contributions to the Pauli repulsion computed from Eq. (13) for the ^{16}O+^{208}Pb system.

Focusing on the differential roles of protons and neutrons in the dynamic rearrangement of net PKE, depicted in Figs. 5 and 6, we find uniform behavior in symmetric reactions (^{40}Ca+^{40}Ca and ^{48}Ca+^{48}Ca), with neutrons presenting a marginally stronger repulsion at shorter distances. Conversely, in asymmetric collisions (^{40}Ca+^{48}Ca and ^{16}O+^{208}Pb), protons exhibit a pronounced increase in net PKE, while neutrons show minimal or even attractive contributions, particularly in the ^{16}O+^{208}Pb interaction. Dynamically, the primary distinction between symmetric and asymmetric encounters is the activation of nucleon transfer channels in the latter, spurred by N/Z equilibra-

tion across nuclei. This quick process, unfolding over approximately 1 zs, initiates upon nuclear contact [15]. Expected are proton transfers from lighter ($N = Z$) to heavier ($N > Z$) nuclei, with neutrons moving oppositely, aligning with experimental observations. The Pauli exclusion principle hinders protons from occupying already filled states, potentially explaining the amplified net PKE due to proton dynamics. Conversely, neutrons may transfer to vacant states without contravening the Pauli principle, suggesting no significant PKE increase. This hypothesis could be further explored using TDHF to microscopically analyze the transfer's initial and final states, setting the stage for future investigations.

4 Summary

The significance of the Pauli exclusion principle in formulating and refining models to compute the interaction between two nuclei has been a focal point of research for a long time. This interest stems from the observation that the effects of antisymmetrization were often considered secondary in many computational strategies. Moreover, there has been debate over the minimal impact of such effects at the peak of the interaction barrier. Contrary to initial beliefs, deviations from this assumption were first recognized in alpha-nucleus potentials and later in scenarios involving higher bombardment energies or energies significantly below the barrier. Attempts to address these discrepancies have ranged from straightforward antisymmetrization of nuclear states—requiring normalization due to the non-representation of lowest energy configurations—to adopting empirically modified shallow potential models that incorporate tailored potential wells.

Here, the novel DCFHF methodology has been applied to derive pure nucleus-nucleus potentials in reactions involving ^{40,48}Ca+^{40,48}Ca and ^{16}O+^{208}Pb. This technique comprehensively incorporates antisymmetrization while optimizing the system's energy by adjusting orbitals against a static density framework. A key feature of the DCFHF approach is its precise adherence to the Pauli exclusion principle (at a mean-field approximation level) without necessitating additional parameters beyond those used in constructing the Skyrme EDF for the nuclear mean-field. Compared to traditional FHF methods, which overlook the Pauli exclusion among nucleons from different nuclei, DCFHF allows for the quantification of Pauli-induced nuclear repulsion, effectively broadening and elevating the interaction barrier to impede fusion below the barrier.

In our research, we've utilized the expression for Pauli kinetic energy derived from nuclear localization function studies within density functional theory. This reveals that repulsion predominantly arises in the fragment's connecting region at distances matching the barrier's radius. Analyzing the Pauli kinetic energy distribution further allows for the dissection of its proton and neutron components, highlighting a dominant neutron effect within neutron-rich systems, thereby proposing additional resistance to sub-barrier fusion in such contexts.

Explorations into the dynamic behaviors of Pauli kinetic energy using the DC-TDHF method have unveiled that the system tends to navigate towards minimizing Pauli repulsion near the barrier. Inside the barrier, though, dynamic processes generally elevate the Pauli kinetic energy as nuclei combine and nucleons undergo collectivization. Notably, the dynamical contributions of protons and neutrons to the Pauli kinetic energy significantly diverge in the examined asymmetric systems, interpreted as a result of multinucleon transfer propelled by swift N/Z balancing. The potential for states transfer with favorable Q-values to mitigate Pauli repulsion highlights a complex interplay that could enhance tunneling probabilities within the Coulomb barrier.

Looking ahead, investigations will focus on the role of Pauli repulsion in mid-shell nuclei to understand better the influences of nuclear pairing and deformation. Additionally, delving into the dynamics of single-particle states involved in transfer mechanisms through microscopic analyses could offer invaluable insights into the nuanced relationship between transfer processes and Pauli kinetic energy. A limitation of the current DC-TDHF approach is that it relies on TDHF trajectories above the Coulomb barrier. To investigate the role of dynamics on Pauli kinetic energy at sub-barrier energies, one would need to extend TDHF to account for many-body tunnelling, e.g., with imaginary time-dependent mean-field methods [16,17].

This work has been supported by the U.S. Department of Energy under award numbers DE-SC0013847 (Vanderbilt University) and DE-NA0004074 (NNSA, the Stewardship Science Academic Alliances program) and by the Australian Research Council Discovery Project (project number DP190100256) funding schemes.

References

[1] C. Simenel, A.S. Umar, K. Godbey, M. Dasgupta, D.J. Hinde, Phys. Rev. C **95**, 031601(R) (2017)
[2] P.G. Reinhard, J.A. Maruhn, A.S. Umar, V.E. Oberacker, Phys. Rev. C **83**, 034312 (2011)
[3] T. Li, M.Z. Chen, C.L. Zhang, W. Nazarewicz, M. Kortelainen, Phys. Rev. C **102**, 044305 (2020)
[4] A.S. Umar, C. Simenel, K. Godbey, Phys. Rev. C **104**, 034619 (2021)
[5] V. Yu. Denisov, W. Nörenberg, Eur. Phys. J. A **15**, 375 (2002)
[6] J. Skalski, Phys. Rev. C **76**, 044603 (2007)
[7] Kouhei Washiyama, Denis Lacroix, Phys. Rev. C **78**, 024610 (2008)
[8] Cédric Simenel, Benoit Avez, Intl. J. Mod. Phys. E **17**, 31 (2008)
[9] Lu Guo, Takashi Nakatsukasa, EPJ Web Conf. **38**, 09003 (2012)
[10] K. Vo-Phuoc, C. Simenel, E.C. Simpson, Phys. Rev. C **94**, 024612 (2016)
[11] A.S. Umar, V.E. Oberacker, Phys. Rev. C **74**, 021601(R) (2006)
[12] K. Washiyama, K. Sekizawa, Front. Phys. **8**, 93 (2020)

[13] G. Scamps, Y. Hashimoto, Phys. Rev. C **100**, 024623 (2019)
[14] S. Liu, D. Zhao, C. Rong, T. Lu, S. Liu, J. Chem. Phys. **150**, 204106 (2019)
[15] C. Simenel, K. Godbey, A.S. Umar, Phys. Rev. Lett. **124**, 212504 (2020)
[16] S. Levit, J.W. Negele, Z. Paltiel, Phys. Rev. C **22**, 1979 (1980)
[17] P. McGlynn, C. Simenel, Phys. Rev. C **102**, 064614 (2020)